JOURNAL OF SOLID STATE CHEMISTRY **130,** 302–310 (1997)
ARTICLE NO. SC977378

Thermodynamic Quantities and Defect Structure of $La_{0.6}Sr_{0.4}Co_{1-y}Fe_yO_{3-\delta}$ ($y = 0$–0.6) from High-Temperature Coulometric Titration Experiments

M. H. R. Lankhorst and J. E. ten Elshof

Department of Chemical Technology, Laboratory of Inorganic Materials Science, University of Twente, P.O. Box 217, 7500 AE Enschede, The Netherlands

Received November 25, 1996; in revised form March 4, 1997; accepted March 5, 1997

The partial energies and entropies of O_2 in perovskite-type oxides $La_{0.6}Sr_{0.4}Co_{1-y}Fe_yO_{3-\delta}$ ($y = 0$, 0.1, 0.25, 0.4, 0.6) were determined as a function of nonstoichiometry δ by coulometric titration of oxygen in the temperature range 650–950°C. An absolute reference value of δ was obtained by thermogravimetry in air. The nonstoichiometry at a given oxygen pressure and temperature decreases with iron content y. At low nonstoichiometries the oxygen chemical potential decreases with δ. The observed behavior can be interpreted by assuming random distribution of oxygen vacancies, an electronic structure with both localized donor states on Fe, and a partially filled itinerant electron band, of which the density of states at the Fermi level scales with the Co content. The energy of the Fe states is close to the energy at the Fermi level in the conduction band. The observed trends of the thermodynamic quantities can be interpreted in terms of the itinerant electron model only when the iron content is small. At high values of δ the chemical potential of O_2 becomes constant, indicating partial decomposition of the perovskite phase. The maximum value of δ at which the compositions are single-phase increases with temperature.

1. INTRODUCTION

The $La_{1-x}Sr_xMO_{3-\delta}$ perovskite-type oxides, in which M is a first row transition metal cation, are well-known for their ability to exhibit significant electronic and oxygen ionic conductivity. It is generally accepted that the high ionic conductivity at elevated temperatures is caused by a relatively high concentration (δ) of vacant crystallographic sites in the oxygen sublattice, in conjunction with a high mobility of the regular oxygen ions. The formation of these lattice oxygen vacancies, which have an electrical charge of $+2$ with respect to the surrounding oxygen sublattice, is charge-compensated by a change in the average valency of the transition metal cations M. Gas separation membranes (1–3), oxidation catalysts (4, 5), and electrodes in solid oxide fuel cells and oxygen sensors (6) are possible applications for these materials.

The present paper is intended to provide insight into the oxygen nonstoichiometry characteristics of the $La_{0.6}Sr_{0.4}Co_{1-y}Fe_yO_{3-\delta}$ (LSCF) system ($y = 0$–0.6) at elevated temperatures. For this purpose, changes in δ are measured as a function of oxygen partial pressure and temperature using the method of oxygen coulometric titration. Thermodynamic quantities such as partial molar energy and entropy of oxygen incorporation are determined with this method, whereas thermogravimetry is used to provide an absolute reference value of δ.

The oxygen nonstoichiometry of the end member $La_{0.6}Sr_{0.4}CoO_{3-\delta}$ has been measured as a function of temperature and oxygen partial pressure by coulometric titration (7, 8). The observed trends were in close agreement with results of thermogravimetric (9) and coulometric titration (10) studies on other compositions $La_{1-x}Sr_xCoO_{3-\delta}$. Within the homogeneity region of the perovskite phase, the value of δ at elevated temperatures is seen to increase almost linearly with decreasing $\log p_{O_2}$ (10, 11). This feature has been explained by assuming the conduction electrons to be delocalized, occupying energy levels in a partially filled conduction band (7). In terms of the ZSA framework (12) this band is thought to have mixed O 2*p*–Co 3*d* character (13), which accounts also for the high metallic-like conductivity and low Seebeck coefficient exhibited by $La_{0.6}Sr_{0.4}CoO_{3-\delta}$ (13–16). With a decreasing level of strontium doping in $La_{1-x}Sr_xCoO_{3-\delta}$ a small band gap appears which results in semiconducting properties at room temperature when $x < 0.25$–0.3 (13, 15). However, metallic-like conductivity is still encountered at higher temperatures (15).

Thermogravimetric experiments in a wide range of temperatures and oxygen partial pressures on the other end member $La_{0.6}Sr_{0.4}FeO_{3-\delta}$ (17) indicated that the increase in the nonstoichiometry with decreasing oxygen partial pressure was substantially smaller than in $La_{0.6}Sr_{0.4}CoO_{3-\delta}$ under the same conditions. Moreover, in contrast to $La_{0.6}Sr_{0.4}CoO_{3-\delta}$ an intermediate region was observed in which δ remains almost constant at a level fixed by the

0022-4596/97 $25.00

dopant concentration, i.e., $\delta \approx 1/2\,[Sr'_{La}]$. For compounds $La_{0.75}Sr_{0.25}FeO_{3-\delta}$ and $La_{0.9}Sr_{0.1}FeO_{3-\delta}$ (18) this region was shown to coincide with a minimum in electrical conductivity. To interpret the observed behavior a Mott–Hubbard type of charge disproportionation is thought to occur: $2Fe^{3+} \rightleftarrows Fe^{4+} + Fe^{2+}$. Thus, both the conduction electrons and the holes are localized, giving rise to hopping-type electrical conductivity. The region of constant nonstoichiometry is caused by a change of the dominant charge carrier from Fe^{4+} to Fe^{2+} upon decreasing p_{O_2} which changes the conductivity from *p*-type to *n*-type. On the other hand, data from X-ray absorption spectrometry on $La_{1-x}Sr_xFeO_{3-\delta}$ ($x = 0$–1) (19) suggest that the holes induced by Sr doping are in states of mixed Fe 3*d*–O 2*p* character, in particular for low concentrations of Sr.

In both end members $La_{0.6}Sr_{0.4}CoO_{3-\delta}$ and $La_{0.6}Sr_{0.4}FeO_{3-\delta}$ the oxygen vacancies are assumed to be distributed randomly among energetically equivalent oxygen sites, although there are indications of microdomain formation with ordered oxygen vacancies at high values of δ for $La_{0.6}Sr_{0.4}CoO_{3-\delta}$ (7). A study of the electrical properties and Seebeck coefficients of the system $La_{0.8}Sr_{0.2}Co_{1-y}Fe_yO_{3-\delta}$ ($y = 0$–1) in air (20) showed a maximum (with respect to temperature) in the electrical conductivity of all compositions. The conduction mechanism assumed is that of adiabatic hopping of small polarons. Since the conductivity decreases with increasing iron content, the iron centers are assumed to represent energetically lower small polaron sites than the cobalt centers, although the energy difference is too small to lead to clear trapping of holes on iron at high temperatures.

There is a lack of data about the nonstoichiometry of $La_{0.6}Sr_{0.4}Co_{1-y}Fe_yO_{3-\delta}$. The oxygen deficiency of $La_{0.6}Sr_{0.4}Co_{0.2}Fe_{0.8}O_{3-\delta}$ in air was measured by thermogravimetry using constant heating and cooling rates of 5°C/min and 2°C/min, respectively (21). From the absence of a hysteresis it was concluded that the material was close to its equilibrium oxygen content during the entire measurement. The oxygen content at room temperature, determined by wet-chemical analysis, was found to be essentially stoichiometric. Significant weight loss was observed only above 600°C, up to a relative mass change of about 1.0% at 1200°C, the value of which corresponds to $\delta \approx 0.14$.

The energy band scheme of $La_{0.6}Sr_{0.4}Co_{1-y}Fe_yO_{3-\delta}$ assumed in the present study for the analysis of experimental data is schematically shown in Fig. 1. It essentially features the characteristics of both end members in the sense that a band model, which takes into account the delocalized behavior of electrons as seen in $La_{0.6}Sr_{0.4}CoO_{3-\delta}$, is combined with the presence of localized electronic states due to partial substitution of cobalt with iron. A rigid band approach to the properties of $La_{0.6}Sr_{0.4}Co_{1-y}Fe_yO_{3-\delta}$ is assumed, whereas it is further assumed that the density of states at the Fermi level and the concentration of localized electronic defects scale with the concentrations of cobalt and iron, respectively.

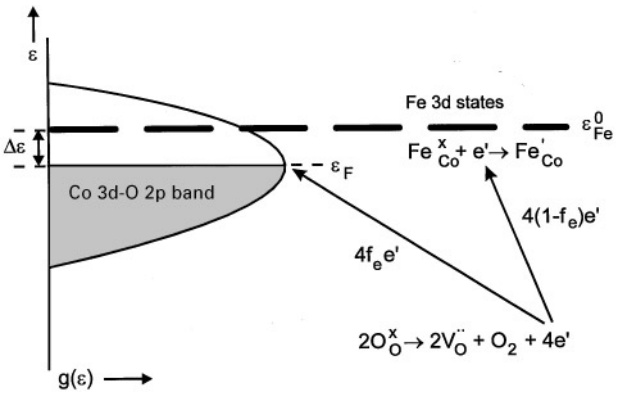

FIG. 1. Schematic representation of the proposed electronic structure of $La_{0.6}Sr_{0.4}Co_{1-y}Fe_yO_{3-\delta}$ and the distribution of electrons created in the oxygen vacancy formation among the band and states.

2. THEORY

2.1. Oxygen Coulometric Titration

The principle of oxygen coulometric titration has been described extensively in Refs. (7, 8). It is performed by placing an oxide sample into a sealed electrochemical cell. In chemical equilibrium the oxygen chemical potential of the oxide sample $\mu_{O_2}^{oxide}$ is equal to that of the surrounding atmosphere inside the cell. Its value is determined by measuring the EMF E across a solid electrolyte wall, onto which two identical metal electrodes are attached on opposite sides, in contact with a reference gas and the atmosphere inside the cell, respectively:

$$\mu_{O_2}^{oxide} = \mu_{O_2}^{ref} - 4FE = \mu_{O_2}^{ref} + RT \ln (p_{O_2}/p_{O_2}^{ref}). \quad [1]$$

Here $\mu_{O_2}^{ref}$ is the oxygen chemical potential of the reference gas. Its value can be found in thermodynamic tables (22). F is Faraday's constant, R the gas constant, and T the temperature. p_{O_2} and $p_{O_2}^{ref}$ are the oxygen partial pressures of the inner atmosphere and the reference gas, respectively. A second auxiliary electrolyte wall in contact with the two gases is used for electrochemical pumping of oxygen into or out of the cell. In potentiostatic coulometric titration experiments the EMF across the electrolyte is changed stepwise from one to another constant value, thus perturbing the equilibrium between the oxide inside the cell and the surrounding atmosphere. The electrical pumping current decays over the time needed for reequilibration. The change in oxygen nonstoichiometry $\Delta\delta$ of the sample follows from integrating the current I over time t:

$$\Delta\delta = \frac{M}{m_s} \int_0^\infty \frac{I(t) - I(\infty)}{2F}\, dt \quad [2]$$

Here $I(\infty)$ is the current at $t = \infty$, which is due to unavoidable leakage of oxygen (7). M is the molar mass of perovskite and m_s the sample mass.

The coulometric titration technique also permits easy determination of the entropy of oxygen $s_{O_2}^{oxide}$ defined as the change of the chemical potential with temperature at constant nonstoichiometry δ (7):

$$s_{O_2}^{oxide} = -\left(\frac{\partial \mu_{O_2}^{oxide}}{\partial T}\right)_{\delta}. \quad [3]$$

The energy of oxygen $\varepsilon_{O_2}^{oxide}$ may be calculated from $\varepsilon_{O_2}^{oxide} = \mu_{O_2}^{oxide} + T s_{O_2}^{oxide}$.

2.2. Solid State Defect Model for $La_{0.6}Sr_{0.4}Co_{1-y}Fe_yO_{3-\delta}$

The creation of oxygen vacancies in $La_{0.6}Sr_{0.4}Co_{1-y}Fe_yO_{3-\delta}$ is assumed to take place in a similar way as in $La_{0.6}Sr_{0.4}CoO_{3-\delta}$ (9) and $La_{0.6}Sr_{0.4}FeO_{3-\delta}$ (17). But in contrast to these compounds it is conjectured that the electrons created during vacancy formation are neither donated exclusively to a partially filled conduction band, like in $La_{0.6}Sr_{0.4}CoO_{3-\delta}$ (7), nor distributed solely among localized electronic states, like in $La_{0.6}Sr_{0.4}FeO_{3-\delta}$. Instead, both processes occur to some extent: a fraction f_e of the electrons formed is donated to the conduction band, while the remaining fraction $1 - f_e$ is distributed among localized states on iron centers. This is illustrated in Fig. 1. It is also assumed that the energy level of Fe^{2+} is too high to be occupied at the oxygen pressures and temperatures covered by our experiments, which leaves Fe^{3+} and Fe^{4+} as the only possible oxidation states. Representing the latter defects in Kröger–Vink notation (23) by Fe'_{Co} and Fe^{x}_{Co}, respectively, the oxidation reaction for a given composition $La_{0.6}Sr_{0.4}Co_{1-y}Fe_yO_{3-\delta}$ can be written as

$$2O_O^x + 4(1-f_e)\,Fe_{Co}^x \rightleftarrows O_2^{gas} + 2V_O^{\bullet\bullet} + 4f_e\,e' + 4(1-f_e)\,Fe'_{Co}. \quad [4]$$

O_O^x denotes a regular lattice oxygen ion, $V_O^{\bullet\bullet}$ an oxygen vacancy, and e' a conduction electron. The exchange of electronic charge carriers between the band and the localized iron states is described by

$$Fe_{Co}^x + e' \rightleftarrows Fe'_{Co}. \quad [5]$$

It follows from these defect reactions that at chemical equilibrium

$$\mu_{O_2}^{oxide} + 2(\mu_{V_O^{\cdot\cdot}} - \mu_{O_O^x}) + 4f_e\mu_{e'} + 4(1-f_e)(\mu_{Fe'_{Co}} - \mu_{Fe^x_{Co}}) = 0 \quad [6]$$

$$(\mu_{Fe_{C_o'}} - \mu_{Fe^x_{Co}}) - \mu_{e'} = 0 \quad [7]$$

where μ_i is the chemical potential of species i. The oxygen vacancies and regular lattice ions are assumed to be noninteracting and randomly distributed among equivalent oxygen sites. A similar assumption is made for the electrons on iron centers. This allows their respective structure elements to be described as

$$\mu_{V_O^{\cdot\cdot}} - \mu_{O_O^x} = \mu_V = \mu_V^0 + RT \ln\left(\frac{\delta}{3-\delta}\right) \quad [8]$$

$$\mu_{Fe'_{Co}} - \mu_{Fe^x_{Co}} = \mu_{Fe} = \mu_{Fe}^0 + RT \ln\left(\frac{[Fe'_{Co}]}{y - [Fe'_{Co}]}\right). \quad [9]$$

By definition, the concentrations of defect species are expressed per unit cell. $[V_O^{\bullet\bullet}] = \delta$ is the oxygen vacancy concentration. $\mu_i = \varepsilon_i - Ts_i$ is the chemical potential of species i, with ε_i and s_i its energy and entropy parts, respectively. $\mu_i^0 = \varepsilon_i^0 - Ts_i^0$ is the standard chemical potential of species i. Under the assumption that the electron band is rigid upon filling with electrons, an expression has been derived for $La_{1-x}Sr_xCoO_{3-\delta}$ (7) which relates $\mu_{e'}$ to the electron occupancy $[e']$ and the density of states at the Fermi level $g(\varepsilon_F)$. The entropy of electrons can be neglected in the description since the electron band is assumed to be relatively wide. Furthermore, due to the wide band nature of the conduction band, $g(\varepsilon_F)$ may be assumed constant as a first order of approximation. Hence, $\mu_{e'}$ is proportional to $[e']$ in $La_{1-x}Sr_xCoO_{3-\delta}$.

For the conduction band of the compounds under investigation here, the density of states at the Fermi level is assumed to be proportional to the concentration $1 - y$ of cobalt. An expression similar to that derived in Ref. (7) can be used for the electron chemical potential in the conduction band in $La_{0.6}Sr_{0.4}Co_{1-y}Fe_yO_{3-\delta}$:

$$\mu_{e'} = \mu_{e'}^0 + \frac{[e'] - [e']^0}{g(\varepsilon_F)(1-y)}. \quad [10]$$

$\mu_{e'}^0$ is the chemical potential of electrons when $\delta = 0$, $y = 0$ and $[Sr'_{La}] = x = 0$, i.e., the chemical potential of electrons in stoichiometric $LaCoO_3$. $[e']^0$ is the electron occupancy under these standard conditions and corresponds to an average valency of 3+ for Co. The charge neutrality requirement for this system may now be written as $2\delta + y = x + n + [Fe'_{Co}]$, with $n = [e'] - [e']^0$.

The value of f_e can be determined by considering that Eq. [7] must still be valid after addition and distribution of the electrons created during oxygen vacancy formation, from which it follows that

$$\left(\frac{\partial \mu_{e'}}{\partial n}\right)_T f_e = \left(\frac{\partial \mu_{Fe}}{\partial [Fe'_{Co}]}\right)_T (1 - f_e). \quad [11]$$

Combining the above equation with Eqs. [9] and [10], f_e can be derived to be

$$f_e = \left(1 + \frac{[Fe'_{Co}]\,(y - [Fe'_{Co}])}{g(\varepsilon_F)(1-y)\,RTy}\right)^{-1}. \qquad [12]$$

In view of Eq. [6], the energy of oxygen $\varepsilon_{O_2}^{oxide}$ may be written as $\varepsilon_{O_2}^{oxide} = -2\varepsilon_V - 4f_e\varepsilon_{e'} - 4(1-f_e)\varepsilon_{Fe}$. Using Eqs. [8]–[10] it then follows that

$$\varepsilon_{O_2}^{oxide} = -2\varepsilon_V^0 - 4f_e\left(\varepsilon_{e'}^0 + \frac{n}{g(\varepsilon_F)(1-y)}\right) - 4(1-f_e)\varepsilon_{Fe}^0$$

$$= \varepsilon_{ox} - 4f_e\left(\frac{n}{g(\varepsilon_F)(1-y)}\right) - 4(1-f_e)\,\Delta\varepsilon_i^0, \qquad (13)$$

where $\varepsilon_{ox} = -2\varepsilon_V^0 - 4\varepsilon_{e'}^0$ is constant for a given iron concentration y. $\Delta\varepsilon_i^0 = \varepsilon_{Fe}^0 - \varepsilon_{e'}^0$ is constant independent of composition, because ε_{Fe}^0 indicates the energy of the $3d$ state of iron, which can be assumed constant, and $\varepsilon_{e'}^0$ is the energy at the Fermi level in stoichiometric $LaCoO_3$. Note, however, that the energy difference $\varepsilon_{Fe}^0 - \varepsilon_{e'}$ scales with the electron occupancy n.

Following the same procedure as above, the entropy of oxygen $s_{O_2}^{oxide}$ may be evaluated from Eq. [6]: $s_{O_2}^{oxide} = -2s_V - 4f_e s_{e'} - 4(1-f_e)s_{Fe}$. Making the appropriate substitutions for s_V, $s_{e'}$, and s_{Fe}, it is found that

$$s_{O_2}^{oxide} = -2\left(s_V^0 - R\ln\frac{\delta}{3-\delta}\right) - 4f_e s_{e'}^0 - 4(1-f_e)$$

$$\times\left(s_{Fe}^0 - R\ln\frac{[Fe'_{Co}]}{y - [Fe'_{Co}]}\right) \qquad [14]$$

$$= s_{ox} + 2R\ln\frac{\delta}{3-\delta} - 4(1-f_e)\left(\Delta s_i^0 - R\ln\frac{[Fe'_{Co}]}{y-[Fe'_{Co}]}\right),$$

where $s_{ox} = -2s_V^0 - 4s_{e'}^0$ and $\Delta s_i^0 = s_{Fe}^0 - s_{e'}^0$ are constants. The latter value can be roughly estimated if possible vibrational contributions to the entropy are neglected. The entropy of electrons in the wide band can be assumed negligible, i.e., $s_{e'}^0 \approx 0$ (24). s_{Fe}^0 represents the difference in entropy between the $3d^5$ (Fe^{3+}) and $3d^4$ (Fe^{4+}) states due to differences in degeneracy v of the magnetic state. The latter difference may be evaluated using a procedure analogous to that used by Korotin *et al.* (25). The total spin in the high spin configuration of $3d^5$ and $3d^4$ states are $S = 5/2$ and $S = 2$, respectively. Thus, their corresponding spin multiplicities $(2S+1)$ are 6 and 5, respectively. As the configuration in $3d^4$ is $t_{2g}^3\,e_g$, either one of the e_g orbitals will remain empty, which increases the total number of possible microstates for Fe^{4+} by another factor of 2. Thus, $v = 6$ for Fe^{3+} ($t_{2g}^3 e_g^2$) and $v = 10$ for Fe^{4+}. Hence $\Delta s_i^0 = s_{Fe}^0 = R\ln(6/10) = -4.25\ \mathrm{J\,mol^{-1}\,K^{-1}}$.

It should be noted that the defect model presented here incorporates the itinerant electron model proposed for $La_{1-x}Sr_xCoO_{3-\delta}$ as a limiting case. If $y = 0$ and $f_e = 1$ are substituted into Eqs. [13] and [14], the results are the same as described previously (7,8). That is, when the concentration y of iron reaches zero, all electrons formed will necessarily go into the conduction band.

3. EXPERIMENTAL

3.1. Sample Preparation

All powders were prepared by thermal decomposition of metal nitrate solutions containing a complexing agent. The EDTA method (6) was applied for making compositions with Fe-dopant levels $y = 0$, 0.1, 0.25, and 0.4, and the citrate synthesis (4) was used for the composition with $y = 0.6$. After calcination in stagnant air at 925°C for 8 h and thorough milling, the powders were pressed uniaxially into cylindrical pellets, followed by isostatic pressing at 4000 bar. The pellets were then sintered in air at 1200°C for 12–18 h. The densities of the resulting disks, expressed relative to theoretical, were 96–98% for all compositions. Phase analysis by means of XRD revealed single-phase perovskite-type oxides (26). Cylindrical samples 7.75 mm in diameter and 3 mm thick were cut from the disks for the experiments. The samples with $y = 0.4$ and $y = 0.6$ were pretreated for 3 h in 2 *M* HNO_3 to enhance the surface exchange kinetics (27).

3.2. Coulometric Titration Experiments

The electrochemical cell in which the measurements were performed has been described in detail elsewhere (7, 8). A $La_{0.6}Sr_{0.4}Co_{1-y}Fe_yO_{3-\delta}$ disk was enclosed in an electrochemical cell with a volume of approximately 250 mm^3. $Zr_{0.87}Y_{0.13}O_{1.935}$ solid electrolytes were used for pumping oxygen into or out of the cell and for the EMF measurements. The reference gas used was air ($p_{O_2} = 0.209$ bar) and the temperature range in which experiments were performed was 650–950°C. Two types of experiments were performed. In the first type, later referred to as voltage step measurements, the equilibrium between oxide and ambient in the cell was perturbed by a stepwise change of the imposed EMF across the electrolyte, after which the decay current $I(t)$ was monitored. After a new equilibrium was reached, i.e., $I(t) = I(\infty)$, the oxygen chemical potential $\mu_{O_2}^{oxide}$ and the nonstoichiometry change $\Delta\delta$ were calculated using Eqs. [1] and [2], respectively.

In the second type of experiments, referred to as temperature step measurements, the open cell EMF was measured at different temperatures at a fixed value of δ. From the

temperature variation of $\mu_{O_2}^{oxide}$ its entropy and energy parts were determined using Eq. [3]. Both heating and cooling steps were applied and the results were averaged. A temperature step measurement was also performed between two isothermal series of voltage step measurements in order to relate their respective δ–p_{O_2} curves.

3.3. Thermogravimetric and Wet-Chemical Analysis

The nonstoichiometry of $La_{0.6}Sr_{0.4}CoO_{3-\delta}$ at room temperature (δ_{RT}) was determined using the oxidizing power method (28) described in more detail by Stevenson *et al.* (21). Prior to analysis the $La_{0.6}Sr_{0.4}CoO_{3-\delta}$ powder was heated to 1000°C and slowly cooled in air (144°C/day) to room temperature. The powder was dissolved in concentrated HCl. Irrespective of the original oxidation state, all Fe and Co will be reduced by the available Cl^- to their $3+$ and $2+$ oxidation states, respectively. The amount of Cl_2 which developed in the reduction process was transported to a KI solution, where it oxidized I^- to I_2. The amount of iodine was determined by titration with $Na_2S_2O_3$, from which the average valency of the transition metal cations was calculated.

For the thermogravimetric (TG) analyses about 200 mg of $La_{0.6}Sr_{0.4}Co_{1-y}Fe_yO_{3-\delta}$ powder was weighed and placed in a platinum cup in a Setaram Microbalance MTB 10-8. Before measurements were made, the powder was heated in air to 900°C to remove traces of impurities, followed by slow cooling to room temperature (0.5–1°C/min) to ensure chemical equilibrium with the ambient oxygen pressure. The powder was then heated with 5–10°C/min in air to several temperatures in the range where coulometric titration experiments had been performed. After equilibration of the sample the weight loss from room temperature was measured, from which the nonstoichiometry change was calculated. Finally the sample was slowly cooled (2–3°C/min) to room temperature. No significant weight change was observed between room temperature and 900°C in a reference measurement on α-Al_2O_3 under the same conditions.

4. RESULTS AND DISCUSSION

4.1. Nonstoichiometry in Air

The chemical analysis of $La_{0.6}Sr_{0.4}CoO_{3-\delta}$ was complicated by the presence of a small amount of carbon (0.13 ± 0.03 mass%) in the powder. Cl_2 formed in the redox reaction may possibly react with it, forming chlorinated hydrocarbons, and thus remain undetected in the iodometric titration. The latter effect reduces the accuracy of the experiments. Still, the result indicated an oxygen concentration close to stoichiometric, i.e., $\delta_{RT} = 0.00 \pm 0.02$. This is consistent with the results of Mizusaki *et al.* (9), who determined the oxygen contents of $La_{0.5}Sr_{0.5}CoO_{3-\delta}$ and $La_{0.7}Sr_{0.3}CoO_{3-\delta}$ at room temperature to be stoichiometric or very close to it. As it may be assumed safely that δ decreases with increasing iron content at a given oxygen pressure and temperature, the other compositions will also be close to stoichiometric.

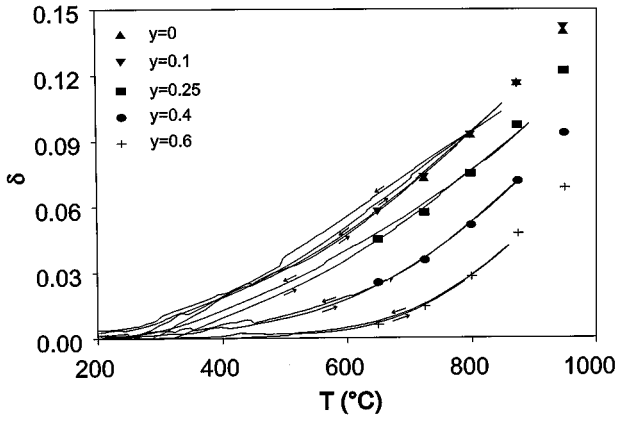

FIG. 2. Nonstoichiometry of $La_{0.6}Sr_{0.4}Co_{1-y}Fe_yO_{3-\delta}$ in air. Drawn lines indicate results of TG analysis using heating and cooling rates of 5 and 2°C/min, respectively. Symbols represent best fits of coulometric titration results to TG curves.

The results of the thermogravimetric analyses in air are indicated in Fig. 2 by the drawn lines. Depending on composition, the onset of weight loss was observed at temperatures of 150–400°C. All weight changes were reversible and independent of cooling rate in the range 0.5–2.5°C/min. Based on these observations and the iodometric titration result, it is concluded that all investigated compositions are stoichiometric at room temperature within experimental error.

For all compositions, the data from coulometric titration experiments at $p_{O_2} = 0.21$ bar were fitted to the TG curves by freely varying the absolute value of the nonstoichiometry at 800°C. The best fits are indicated by the symbols in Fig. 2. The values for δ obtained from fitting are listed in Table 1. A value $\delta \approx 0.023$ has been determined for $La_{0.6}Sr_{0.4}Co_{0.2}Fe_{0.8}O_{3-\delta}$ under the same conditions (21), which agrees

TABLE 1
Absolute Nonstoichiometries of $La_{0.6}Sr_{0.4}Co_{1-y}Fe_yO_{3-\delta}$ at 800°C in Air Determined by TGA

y	δ (800°C, air)
0	0.093
0.1	0.093
0.25	0.075
0.4	0.052
0.6	0.028

Note. Absolute error $\Delta\delta = \pm 0.003$.

reasonably with that obtained from extrapolation of the present results.

4.2. Thermodynamic Stability of the $La_{0.6}Sr_{0.4}Co_{0.75}Fe_{0.25}O_{3-\delta}$ Phase

The partial thermodynamic quantities $\varepsilon_{O_2}^{oxide}$ and $s_{O_2}^{oxide}$ of $La_{0.6}Sr_{0.4}Co_{0.75}Fe_{0.25}O_{3-\delta}$ obtained from temperature step measurements in the range 650–950°C are shown in Fig. 3a. The range of nonstoichiometries covered by the experiments is $\delta = 0.066$–0.364. Two different regions can be distinguished within this range. In the region where $\delta < 0.20$ the general trends are more or less similar to those observed previously on $La_{0.8}Sr_{0.2}CoO_{3-\delta}$ (8). This range of nonstoichiometries will be discussed in more detail below.

The region $\delta > 0.20$ is characterized by an increasing partial energy $\varepsilon_{O_2}^{oxide}$ with δ, while the entropy of oxygen $s_{O_2}^{oxide}$ increases much more strongly than in the region $\delta < 0.20$. At very high values of δ both quantities tend to become constant. The change in slope of $\varepsilon_{O_2}^{oxide}$ at $\delta = 0.20$–0.25 cannot be explained in terms of randomly distributed, noninteracting defects.

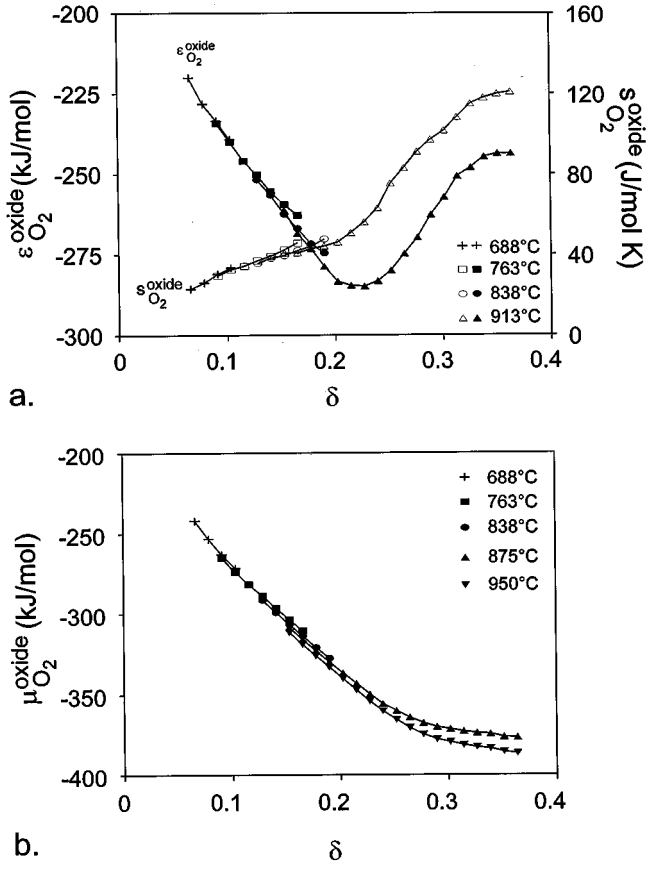

FIG. 3. Experimental energy $\varepsilon_{O_2}^{oxide}$ and entropy $s_{O_2}^{oxide}$ of oxygen in $La_{0.6}Sr_{0.4}Co_{0.75}Fe_{0.25}O_{3-\delta}$.

The chemical potential of oxygen $\mu_{O_2}^{oxide} = \varepsilon_{O_2}^{oxide} - Ts_{O_2}^{oxide}$ is shown in Fig. 3b. A change in behavior is clearly observed at higher values of δ. In the region $\delta = 0.20$–0.25 the change in slope of $\varepsilon_{O_2}^{oxide}$ can still be compensated by the increasing slope of $s_{O_2}^{oxide}$. At higher values of δ the oxygen chemical potential appears to reach a constant value, which indicates a chemical equilibrium between two or more phases.

Petrov *et al.* (10, 16) showed by combined coulometric titration and XRD experiments that $La_{0.7}Sr_{0.3}CoO_{3-\delta}$ decomposes into $La_{1.4}Sr_{0.6}CoO_{4\pm\nu}$, $Co_{1-y}O$, and O_2 at a sufficiently high value of δ. A similar kind of decomposition reaction may occur in $La_{0.6}Sr_{0.4}Co_{0.75}Fe_{0.25}O_{3-\delta}$. The limit of thermodynamic stability in $La_{0.7}Sr_{0.3}CoO_{3-\delta}$ moves to higher values of δ with increasing temperature (10). This is consistent with the results in Fig. 3b, where the O_2 chemical potential becomes constant at a slightly higher value of δ with increasing temperature.

It should be noted that the onset of decomposition occurs at a value near $\delta = 1/2[Sr'_{La}]$, the nonstoichiometry at which the average valency of all transition metal cations is exactly $3+$. Similar features were observed in the same region of nonstoichiometries on all other compositions containing iron. Attention will be focused on the region $\delta < 0.20$ in the remainder of this study.

4.3. Partial Thermodynamic Quantities of $La_{0.6}Sr_{0.4}Co_{1-y}Fe_yO_{3-\delta}$

As stated already the overall features observed in Fig. 3a in the region $\delta < 0.2$ are similar to those observed on $La_{0.8}Sr_{0.2}CoO_{3-\delta}$ (7, 8). $\varepsilon_{O_2}^{oxide}$ is seen to decrease almost linearly with δ, while $s_{O_2}^{oxide}$ is logarithmically dependent on δ to a first order of approximation. Both features can be understood in terms of the itinerant electron model, which has been applied successfully to describe $La_{0.8}Sr_{0.2}CoO_{3-\delta}$, as well as $La_{0.6}Sr_{0.4}CoO_{3-\delta}$ and $La_{0.3}Sr_{0.7}CoO_{3-\delta}$ at high temperature and small δ (7, 8). According to this model, the decrease of $\varepsilon_{O_2}^{oxide}$ is linear due to the filling of the conduction band with electrons upon creation of oxygen vacancies, while $s_{O_2}^{oxide}$ increases with δ because of the increasing configurational entropy of oxygen $s_{conf} = 2R\ln(\delta/(3-\delta))$. The same contributions also emerge in the defect model proposed for LSCF in Section 2.2. The argument of discussion given below is that for small values of y the itinerant electron model gives a fair description of the nonstoichiometry behavior of LSCF, but this model no longer holds at high iron substitution levels.

This agreement at small value of y can be clearly illustrated by the thermodynamic quantities of $La_{0.6}Sr_{0.4}Co_{0.9}Fe_{0.1}O_{3-\delta}$, shown in Fig. 4. Note that these data exhibit the same trends as observed on $La_{0.6}Sr_{0.4}Co_{0.75}Fe_{0.25}O_{3-\delta}$ as shown in Fig. 3. The drawn lines in Fig. 4 are the best fits of Eqs. [13] and [14] to the experimental data. The corresponding values of ε_{ox}, s_{ox} and $\Delta\varepsilon_i^0$ are listed in Table 2. It

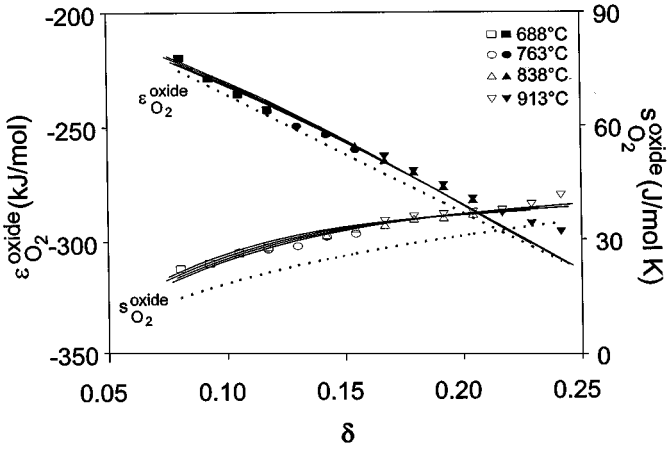

FIG. 4. Energy $\varepsilon_{O_2}^{oxide}$ and entropy $s_{O_2}^{oxide}$ of oxygen in $La_{0.6}Sr_{0.4}Co_{0.9}Fe_{0.1}O_{3-\delta}$. Experimental results are indicated by symbols; best fits of LSCF model indicated by drawn lines; trends according to itinerant electron model indicated by broken lines.

should be noted that since $\Delta\varepsilon_i^0$ is assumed to be independent of iron content, its value was determined by optimization of curve fits to data of other compositions as well. The value $g(\varepsilon_F) = 1.47\ eV^{-1}$, determined from the best fit of Eq. [13] to the data of $La_{0.6}Sr_{0.4}CoO_{3-\delta}$, was adopted for all compositions. This value is close to $g(\varepsilon_F) = 1.53\ eV^{-1}$ reported previously for $La_{0.6}Sr_{0.4}CoO_{3-\delta}$ (7). For the sake of clarity, the values of ε_{ox} and s_{ox} from Table 2 were used to draw the broken lines in Fig. 4, which indicate the predictions according to the itinerant electron model. Very close agreement is obtained if the latter values are adjusted to $\varepsilon_{ox} = -281$ kJ/mol and $s_{ox} = 82$ J/mol K. Hence, it is concluded that the thermodynamics of $La_{0.6}Sr_{0.4}Co_{0.9}Fe_{0.1}\ O_{3-\delta}$ can be understood both within the framework of the itinerant electron model and the proposed defect model for LSCF. Next to the small iron content, close agreement between the models is also due to the small energy difference between the 3*d* states of iron and the energy at the Fermi level. The value $\Delta\varepsilon_i^0 = -25$ kJ/mol indicates a small energy difference between the Fermi level of $LaCoO_3$ and the e_g state of Fe of about 0.25 eV. The difference becomes even smaller upon doping $LaCoO_3$ with strontium, due to the downward shift of the Fermi level. This implies that trapping of electron holes by Fe 3*d* states will not occur. These results are essentially in agreement with the findings of Tai *et al.* (20). Large differences between the predictions of both models will occur only at large concentrations of iron, as will be discussed in more detail below for the case of $La_{0.6}Sr_{0.4}Co_{0.4}Fe_{0.6}O_{3-\delta}$.

It is interesting to note that deviations from the behavior predicted by the itinerant electron model occur at much lower values of δ in $La_{0.6}Sr_{0.4}CoO_{3-\delta}$ (7) than in $La_{0.6}Sr_{0.4}Co_{0.9}Fe_{0.1}O_{3-\delta}$. In $La_{0.6}Sr_{0.4}CoO_{3-\delta}$ this has been attributed to additional ionic contributions to the partial energy and entropy of oxygen, possibly caused by the formation of microdomains with ordered oxygen vacancies. In contrast, such additional ionic contributions seem not to be apparent in $La_{0.6}Sr_{0.4}Co_{0.9}Fe_{0.1}O_{3-\delta}$ up to large δ. This suggests that substitution of a small amount of Co by Fe may stabilize the random distribution of oxygen vacancies to much higher concentrations.

Figure 5 shows the thermodynamic quantities of $La_{0.6}Sr_{0.4}Co_{0.4}Fe_{0.6}O_{3-\delta}$. Symbols and lines have the same meaning as in the previous figure. Reasonable agreement is obtained between experimental data and best fits of Eqs. [13] and [14], but the itinerant electron model predicts strongly deviating trends, with best fits for $\varepsilon_{ox} \approx -290$ kJ/mol and $s_{ox} = 120$ J/mol K. Note that the values of s_{ox} remain constant within experimental error for the LSCF model.

TABLE 2
Thermodynamic Quantities ε_{ox}, $\Delta\varepsilon_i^0$, s_{ox}, Δs_i^0, and $g(\varepsilon_F)$ Determined from Fitting Eqs. [13] and [14] to the Experimental Data

y	ε_{ox} (kJ/mol)	$\Delta\varepsilon_i^0$ (kJ/mol)	s_{ox} (J/mol K)	Δs_i^0 (J/mol K)	$g(\varepsilon_F)$ ((kJ/mol)$^{-1}$)
0	−281	−25	86	−4.25	0.0153
0.1	−288	−25	75	−4.25	0.0153
0.25	−297	−25	73	−4.25	0.0153
0.4	−305	−25	79	−4.25	0.0153
0.6	−314	−25	83	−4.25	0.0153

4.4. *Nonstoichiometry of $La_{0.6}Sr_{0.4}Co_{1-y}Fe_yO_{3-\delta}$*

The experimental data for the nonstoichiometry of $La_{0.6}Sr_{0.4}Co_{0.9}Fe_{0.1}O_{3-\delta}$ and $La_{0.6}Sr_{0.4}Co_{0.4}Fe_{0.6}O_{3-\delta}$

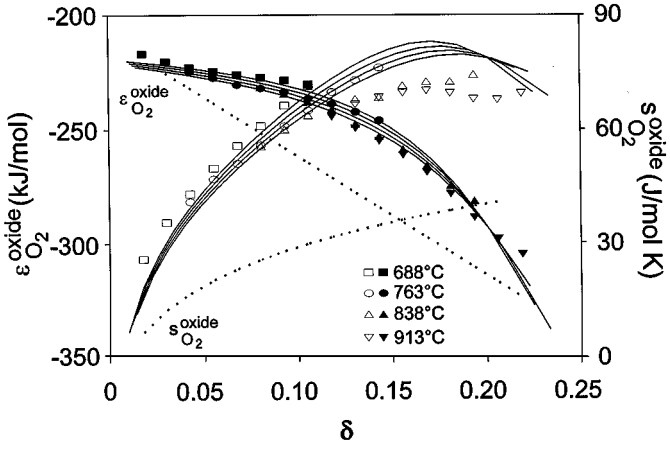

FIG. 5. Energy $\varepsilon_{O_2}^{oxide}$ and entropy $s_{O_2}^{oxide}$ of oxygen in $La_{0.6}Sr_{0.4}Co_{0.4}Fe_{0.6}O_{3-\delta}$. Experimental results are indicated by symbols; best fits of LSCF model indicated by drawn lines; trends according to itinerant electron model indicated by broken lines.

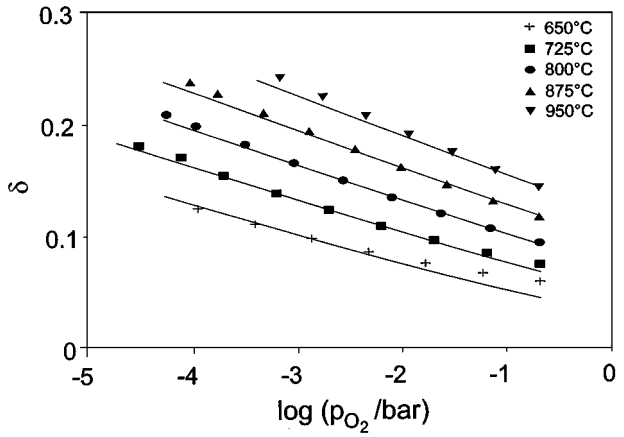

FIG. 6. Nonstoichiometry of $La_{0.6}Sr_{0.4}Co_{0.9}Fe_{0.1}O_{3-\delta}$ versus oxygen partial pressure p_{O_2}. Drawn lines indicate best fits of the LSCF model to the experimental data.

obtained from voltage step measurements are shown in Figs. 6 and 7. The drawn lines are the theoretical curves according to the LSCF model with the values of ε_{ox}, s_{ox}, and $\Delta\varepsilon_i^0$ determined from the temperature step measurements inserted. The good agreement supports the correctness of the energy band scheme proposed in Fig. 1 for modeling the data of oxygen nonstoichiometry of compositions $La_{0.6}Sr_{0.4}Co_{1-y}Fe_yO_{3-\delta}$. For $La_{0.6}Sr_{0.4}Co_{0.9}Fe_{0.1}O_{3-\delta}$ deviations from the theoretical curves are observed when $\delta > 0.20$, which is attributed to a limited phase stability as discussed above for $La_{0.6}Sr_{0.4}Co_{0.75}Fe_{0.25}O_{3-\delta}$. Deviations are also observed at 650°C at high oxygen pressure, which is not understood at present.

Excellent agreement is seen between experimental and theoretical curves for $La_{0.6}Sr_{0.4}Co_{0.4}Fe_{0.6}O_{3-\delta}$ in Fig. 7 in the whole temperature and pressure range. It appears from this figure as well as from other data that the LSCF model performs better in representing the defect chemistry of the $La_{0.6}Sr_{0.4}Co_{1-y}Fe_yO_{3-\delta}$ system at higher iron contents.

The observed decrease in δ with y in $La_{0.6}Sr_{0.4}Co_{1-y}Fe_yO_{3-\delta}$ at a given temperature and oxygen pressure can be explained in terms of the defect model by considering that ε_{ox} can be regarded as a measure of the binding strength of O^{2-} in the oxide. Thus, the increase of its absolute magnitude with iron concentration reflects an increasing binding strength, which will suppress oxygen vacancy formation. Furthermore, it can be shown that the average valency of the iron atoms is larger than the average valency of cobalt under all conditions. This indicates that strontium doping is charge-compensated more readily by hole formation on iron than on cobalt. Considering that the hole concentration is negatively proportional to the oxygen vacancy concentration, the presence of iron will lower the nonstoichiometry.

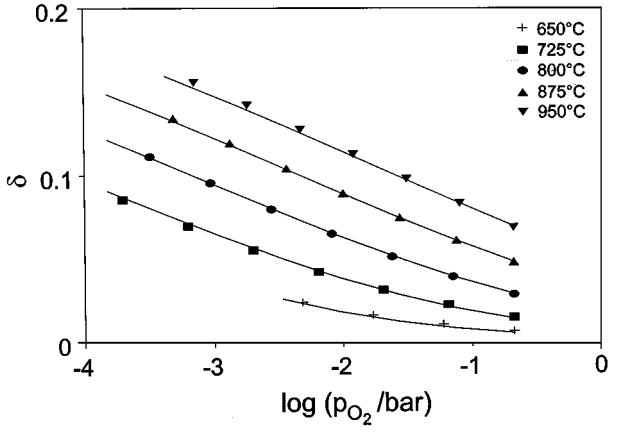

FIG. 7. Nonstoichiometry of $La_{0.6}Sr_{0.4}Co_{0.4}Fe_{0.6}O_{3-\delta}$ versus oxygen partial pressure p_{O_2}. Drawn lines indicate best fits of the LSCF model to the experimental data.

5. CONCLUSIONS

The level of nonstoichiometry δ in perovskites $La_{0.6}Sr_{0.4}Co_{1-y}Fe_yO_{3-\delta}$ decreases with iron content, which is attributed to an increasing binding energy of oxygen O^{2-} in the lattice and a larger tendency of iron to form holes rather than oxygen vacancies. At relatively small values of δ, the energy and entropy of O_2 in the oxide can be interpreted in terms of a new model proposed to describe the defect structure. The oxygen vacancies are thought to be distributed randomly, while the electrons created during oxygen vacancy formation are partly donated to a partially filled electron band, of which the density of states at the Fermi level scales with the Co content, and partly to Fe donor centers. The energy of the latter states is close to the Fermi level energy. The observed trends can only be described satisfactorily in terms of the itinerant electron model at small values of y. The substitution of small amounts of Co by Fe appears to suppress features observed previously on $La_{0.6}Sr_{0.4}CoO_{3-\delta}$ at relatively high δ, attributed to clustering of oxygen vacancies in microdomains. The perovskite phase decomposes partly at high values of δ, but the value of δ at which the onset of decomposition occurs increases with temperature.

ACKNOWLEDGMENTS

J. M. Rietmann is gratefully acknowledged for technical assistance in the TGA experiments. H. J. M. Bouwmeester is gratefully acknowledged for useful discussions.

REFERENCES

1. Y. Teraoka, H.-M. Zhang, S. Furukawa, and N. Yamazoe, *Chem. Lett.* 1743 (1985).

2. L. Qiu, T. H. Lee, L.-M. Liu, Y. L. Yang, and A. J. Jacobsen, *Solid State Ionics* **76,** 321 (1995).
3. J. E. ten Elshof, H. J. M. Bouwmeester, and H. Verweij, *Solid State Ionics* **81,** 97 (1995).
4. H. M. Zhang, Y. Shimizu, Y. Teraoka, N. Miura, and N. Yamazoe, *J. Catal.* **121,** 432 (1990).
5. J. E. ten Elshof, H. J. M. Bouwmeester, and H. Verweij, *Appl. Cat. A* **130,** 195 (1995).
6. H. J. M. Bouwmeester, *in* "CRC Handbook Solid State Electrochemistry" (P. J. Gellings and H. J. M. Bouwmeester, Eds.), p. 481–553. CRC Press, Boca Raton, FL, 1996.
7. M. H. R. Lankhorst, "Thermodynamic and Transport Properties of Mixed Ionic-Electronic Conducting Perovskite-Type Oxides," pp. 103–122. Thesis, University of Twente, Enschede, The Netherlands, 1997; M. H. R. Lankhorst, H. J. M. Bouwmeester, and H. Verweij, *Solid State Ionics*, in press (1997).
8. M. H. R. Lankhorst, H. J. M. Bouwmeester, and H. Verweij, *Phys. Rev. Lett.* **77**, 2989 (1996).
9. J. Mizusaki, Y. Mima, S. Yamauchi, K. Fueki, and H. Tagawa, *J. Solid State Chem.* **80,** 102 (1989).
10. A. N. Petrov, V. A. Cherepanov, O. F. Kononchuk, and L. Ya. Gavrilova, *J. Solid State Chem.* **87,** 69 (1990).
11. V. A. Cherepanov, L. Yu. Barkhatova, A. N. Petrov, and V. I. Voronin, "Proc. 2nd Symp. on Solid Oxide Fuel Cells" (M. Dokiya, O. Yamamoto, H. Tagawa, and S. C. Singhal, Eds.), The Electrochemical Society Proceedings Series PV 95-1, pp. 434–443. The Electrochemical Society, Pennington, NJ, 1995.
12. J. Zaanen, G. A. Sawatzky, and J. W. Allen, *Phys. Rev. Lett.* **55,** 418 (1985).
13. A. Mineshige, M. Inaba, T. Yao, Z. Ogumi, K. Kikuchi, and M. Kasawe, *J. Solid State Chem.* **121,** 423 (1996).
14. M. H. R. Lankhorst, "Thermodynamic and Transport Properties of Mixed Ionic-Electronic Conducting Perovskite-Type Oxides," pp. 73–86. Thesis, University of Twente, Enschede, The Netherlands, 1997.
15. J. Mizusaki, J. Tabuchi, T. Matsuura, S. Yamauchi, and K. Fueki, *J. Electrochem. Soc.* **136,** 2082 (1989).
16. A. N. Petrov, O. F. Kononchuk, A. V. Andreev, V. A. Cherepanov, and P. Kofstad, *Solid State Ionics* **80,** 189 (1995).
17. J. Mizusaki, M. Yoshihiro, S. Yamauchi, and K. Fueki, *J. Solid State Chem.* **58,** 257 (1985).
18. J. Mizusaki, T. Sasamoto, W. R. Cannon, and H. K. Bowen, *J. Am. Ceram. Soc.* **66,** 247 (1983).
19. M. Abbate, F. M. F. de Groot, J. C. Fuggle, A. Fujimori, O. Strebel, F. Lopez, M. Domke, G. Kaindl, G. A. Sawatzky, M. Takano, Y. Takeda, H. Eisaki, and S. Uchida, *Phys. Rev. B* **46,** 4511 (1992).
20. L.-W. Tai, M. M. Nasrallah, H. U. Anderson, D. M. Sparlin, and S. R. Sehlin, *Solid State Ionics* **76,** 259 (1995).
21. J. W. Stevenson, T. R. Armstrong, R. D. Carneim, L. R. Pederson, and W. J. Weber, *J. Electrochem. Soc.* **143,** 2722 (1996).
22. IUPAC, Commission on Thermodynamics; "Oxygen, International Thermodynamic Tables of the Fluid State-9," Blackwell Sci., Oxford, 1987.
23. F. A. Kröger, "The Chemistry of Imperfect Crystals," North-Holland, Amsterdam, 1964.
24. M. H. R. Lankhorst, "Thermodynamic and Transport Properties of Mixed Ionic-Electronic Conducting Perovskite-Type Oxides," Chap. 2. Thesis, University of Twente, Enschede, The Netherlands, 1997.
25. M. A. Korotin, S. Yu. Ezhov, I. V. Solovyev, V. I. Anisimov, D. I. Khomskii, and G. A. Sawatzky, *Phys. Rev. B* **54,** 5309 (1996).
26. J. E. ten Elshof and J. Boeijsma, *Powder Diff.* **11,** 240 (1996).
27. N. Miura, Y. Okamoto, J. Tamaki, K. Morinaga, and N. Yamazoe, *Solid State Ionics* **79**, 195 (1995).
28. R. J. Nadalin and W. Brozda, *Anal. Chim. Acta* **28,** 282 (1963).